Generation of a widely tunable linearly chirped microwave waveform based on spectral filtering and unbalanced dispersion

Hao Zhang,[1] Weiwen Zou,[1,2,*] and Jianping Chen[1,2]

[1]*State Key Laboratory of Advanced Optical Communication Systems and Networks, Department of Electronic Engineering, Shanghai Jiao Tong University, Shanghai 200240, China*

[2]*Shanghai Key Lab of Navigation and Location Services, Shanghai Jiao Tong University, Shanghai 200240, China*

**Corresponding author: wzou@sjtu.edu.cn*

Received January 14, 2015; revised February 5, 2015; accepted February 9, 2015; posted February 11, 2015 (Doc. ID 232417); published March 12, 2015

We propose a method to generate a widely tunable linearly chirped microwave waveform based on spectral filtering and unbalanced dispersion. Heterodyne beating between two differently dispersed optical pulses in a photodetector produces the linearly chirped microwave waveform. Desired waveforms with flexible and independent control of the center frequency and sweep bandwidth can be obtained by simply tuning two optical filters. Simulation and experimental investigations are carried out, and the results are in good agreement. The measured microwave waveform has ~5.2-ns pulse duration and ~64-GHz sweep bandwidth, corresponding to a time–bandwidth product of ~166.4 and a compression ratio of ~248. © 2015 Optical Society of America

OCIS codes: (060.5625) Radio frequency photonics; (140.4050) Mode-locked lasers; (280.5600) Radar; (350.4010) Microwaves.

http://dx.doi.org/10.1364/OL.40.001085

Linearly chirped microwave waveform has been widely used in modern radar systems [1] and optical instruments [2] due to its advantage of high detection accuracy. In principle, the range resolution after the pulse compression is determined by the bandwidth and the pulse compression ratio is proportional to the time–bandwidth product (TBWP) of the microwave waveform [3]. Owing to the inherent characteristics of high speed and broad bandwidth, various photonics-based methods [4,5] have been proposed. The main shortcoming of the methods based on polarization modulation [6] or phase modulation [7] is that external electrical devices are still required. The other methods based on spatial optics [8,9] make the system bulky and complicated. In contrast, methods based on the wavelength-to-time mapping [10–15] are more attractive due to superior tunability. In these methods, the optical spectra of mode-locked laser (MLL) are shaped by a Mach–Zehnder interferometer (MZI) or a Sagnac loop [10–14]. A dispersive element such as a dispersion compensation fiber (DCF), single mode fiber, or chirped FBG is utilized to map the shaped optical spectra to time domain. However, tuning of the generated signal's center frequency via changing the time delay in MZI reduces the pulse duration. Also, tuning of the sweep bandwidth via changing the dispersion values is not easy. In [15], beating of a pre-chirped optical pulse with the CW optical signal can generate linearly chirped microwave waveform with more tuning flexibility. However, the phase irrelevance of two independent lasers may result in unexpected instability.

In this Letter, we present a novel method to generate widely tunable linearly chirped microwave waveform based on spectral filtering and unbalanced dispersion. Both the center frequency and sweep bandwidth of the generated waveforms can be flexibly and independently controlled by tuning two tunable optical filters (TOFs). The measured microwave waveform with ~5.2-ns pulse duration and ~64-GHz sweep bandwidth is demonstrated, corresponding to the TBWP of ~166.4 and compression ratio of ~248. It is rather more competitive than other works [10–15].

Figure 1 shows the schematic of the proposed method. The optical source is a MLL with tens of nanometers bandwidth, which is sufficient for spectral filtering. A 50:50 optical coupler (OC1) divides the optical source into two arms. Their optical spectra are shaped by TOF1 and TOF2 with approximately rectangular profiles. Two sections of DCFs, DCF1, and DCF2 with different dispersions are used to introduce different chirps into the optical pulses via wavelength-to-time mapping effect. A variable optical delay line (VODL) is added in the second arm to adjust the difference of time delay in two arms caused by two DCFs to an integer multiple of the pulse period. It is different from previous methods [10–14] where VODL was used to change the center frequency of generated waveform. After coupled together by another 50:50 optical coupler (OC2) and amplified by an erbium-doped fiber amplifier (EDFA), the optical signal is converted into a linearly chirped microwave waveform by a photodetector (PD).

The ultra-short optical pulse ($|\Delta t_0/2\pi\ddot{\Phi}_i| \ll 1$) experiencing different dispersion chirps through DCFs in two arms can be expressed as [15,16]:

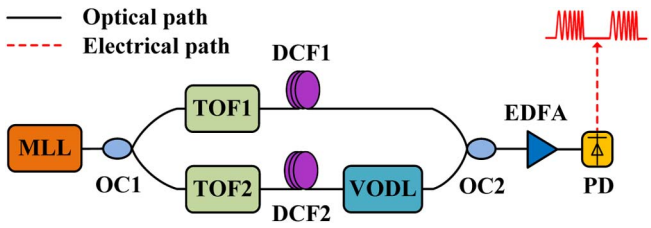

Fig. 1. Schematic of the proposed method. MLL, mode-locked laser; OCs, optical couplers; TOFs, tunable optical filters; DCFs, dispersion compensation fibers; VODL, variable optical delay line; EDFA, erbium-doped fiber amplifier; PD, photodetector.

$$y_i(t) = C_i A_i(t) \exp\left[j\left(\omega_i t + \frac{t^2}{2\ddot{\Phi}_i}\right)\right], \tag{1}$$

with

$$A_i(t) = \{\mathcal{F}[x_i(t)]\}_{\omega-\omega_i=t/\ddot{\Phi}_i}, \tag{2}$$

where C_i is a constant, $\ddot{\Phi}_i$ is the dispersion value of the DCFs, $\mathcal{F}[x_i(t)]$ is the Fourier transform of the filtered optical signal $x_i(t)$ out of TOFs, ω_i is the center angular frequency of the filtered optical pulse, Δt_0 is the temporal width of optical pulses of MLL, t is the time offset from the average time delay t_i, and the subscript of $i = 1$ or 2 corresponds to two arms, respectively. Note that the time delay between the two arms ($\tau = t_1 - t_2$) is kept unchanged as long as it is properly adjusted by VODL to an integer multiple of the pulse period T. When the coupled optical signal after the OC2 is detected by the PD, the output current can be expressed as

$$\begin{aligned} i(t) &= \Re\cdot\{[y_1(t) + y_2(t)]\cdot[y_1(t) + y_2(t)]^*\} \\ &= \Re\cdot\{C_1^2A_1^2(t) + C_2^2A_2^2(t) \\ &\quad + 2C_1C_2A_1(t)A_2(t)\cos[\Phi(t)]\}, \end{aligned} \tag{3}$$

where $\Phi(t) = (\omega_1 - \omega_2)t + \frac{t^2}{2}(\frac{1}{\ddot{\Phi}_1} - \frac{1}{\ddot{\Phi}_2})$, and $\Re$ is the responsibility of the PD. According to the differential relationship between the phase factor and frequency, the instantaneous frequency can be written as

$$f = \frac{\left|\omega_1 - \omega_2 + \left(\frac{1}{\ddot{\Phi}_1} - \frac{1}{\ddot{\Phi}_2}\right)t\right|}{2\pi}, \tag{4}$$

when $t = 0$, the center frequency is determined by

$$f_{\text{center}} = \frac{|\omega_1 - \omega_2|}{2\pi}. \tag{5}$$

Suppose that λ_0 represents the average center wavelengths of TOFs and $\Delta\lambda$ denotes the relatively smaller filtering bandwidth of two TOFs. If ignoring the impact of high-order dispersion, the pulse duration, sweep bandwidth, TBWP, and sweep rate of the generated microwave waveform can be approximated as

$$T_d \approx \frac{|2\pi c\Delta\lambda\ddot{\Phi}_2|}{\lambda_0^2}, \tag{6}$$

$$B \approx \frac{c\Delta\lambda}{\lambda_0^2}\left(1 - \frac{\ddot{\Phi}_2}{\ddot{\Phi}_1}\right), \tag{7}$$

$$\text{TBWP} = T_dB \approx \frac{|2\pi c^2(\Delta\lambda)^2\ddot{\Phi}_2|}{\lambda_0^4}\left(1 - \frac{\ddot{\Phi}_2}{\ddot{\Phi}_1}\right), \tag{8}$$

$$K = \frac{B}{T_d} \approx \frac{\left|\frac{1}{\ddot{\Phi}_1} - \frac{1}{\ddot{\Phi}_2}\right|}{2\pi}. \tag{9}$$

According to the real-time Fourier transform introduced by dispersion [16], the temporal signal amplitude at t is proportional to the Fourier transform of input signal at the angular frequency $\omega = t/\ddot{\Phi}$, which is illustrated in Fig. 2(a). The filtered optical spectra in two arms can be mapped to the temporal waveforms through DCFs. As given in Eq. (6), the pulse duration of the optical pulse is proportional to both the filtering bandwidth of TOF and the dispersion of DCF. The rectangular color bars (i) and (ii) represent different wavelength components beating at the PD at different time when TOF1 and TOF2 have the same filtering bandwidth and center wavelength. Note that (i) experiences more dispersion and hence is longer than (ii). The time axis is the time offset from the middle time in an observation window. For the beating of (i) and (ii), the center frequency at the middle time t_2 is 0 GHz. Color bar (iii) represents the beating wavelength components when the center wavelength of TOF2 is detuned. For the beating between (i) and (iii), the frequency at the middle time t_2' changes accordingly. For the beating between (i) and (iv) when there is a temporal shift between two arms as presented in [10–14], the pulse duration T_{d2} becomes shorter than T_{d1}. In comparison with this method, the sweep bandwidth in [10–14] is correspondingly reduced since the sweep rate is fixed [see Eq. (9)]. The lines in Fig. 2(b) represent the instantaneous frequency at the start, middle, and end time of the microwave waveform when changing the optical frequency offset between two TOFs. Here, suppose total linearly sweep bandwidth is 40 GHz.

Figure 3 shows the numerical simulation on three types of linearly chirped microwave waveforms and their short-time Fourier transform (STFT) analysis when there is optical frequency offset between two TOFs while their filtering bandwidths are the same. The pulse durations are all assumed to be 4 ns. White Gaussian noises with a magnitude determining a signal-to-noise ratio of 30 dB are added to the ideal waveforms. The microwave waveform in Figs. 3(a) and 3(b) is centered at 0 GHz, which can be regarded as a combination of 2-ns down-chirp and 2-ns up-chirp. The maximum instantaneous frequency is 20 GHz. The waveforms in Figs. 3(c) and 3(e) are both centered at 20 GHz, while their chirp directions are opposite. When the center wavelength of TOF2 is larger (smaller) than TOF1, the optical frequency offset is negative (positive). Therefore, the waveform in Fig. 3(c) is down-chirp from 40 to 0 GHz [see Fig. 3(d)] and that in Fig. 3(e) is up-chirp from 0 to 40 GHz [see Fig. 3(f)].

In order to verify the proposed method, we carry out the following experiments. DCF1 and DCF2 have

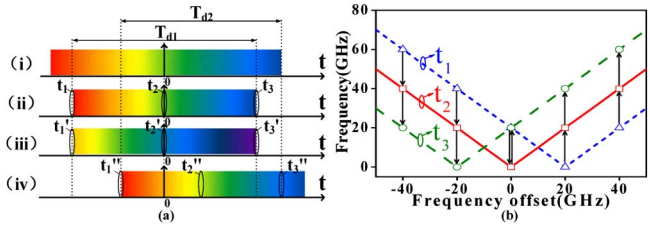

Fig. 2. (a) Principle of the proposed method. (b) Instantaneous frequency at the start, middle, and end time of the microwave waveform when the optical frequency offset between two TOFs is tuned.

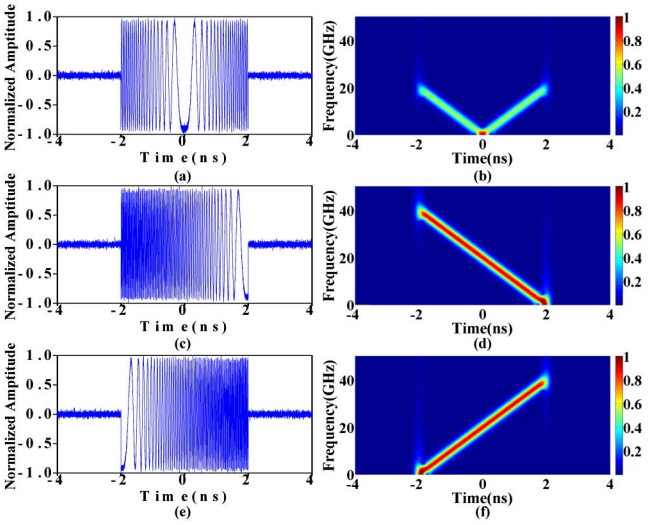

Fig. 3. (a), (c), (e) Temporal waveforms and (b), (d), (f) STFT analyses of the simulated microwave waveforms when tuning optical frequency offset between two TOFs.

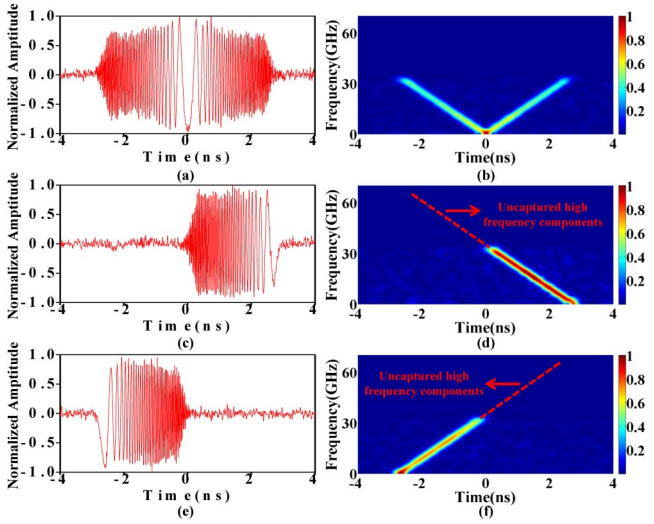

Fig. 5. (a), (c), (e) Temporal waveforms and (b), (d), (f) STFT analyses of the generated microwave waveforms when the center wavelength of the TOF2 is detuned by (a), (b) 0 nm; (c), (d) +0.26 nm; (e), (f) −0.26 nm.

different dispersion values of $\ddot{\Phi}_1 = -1915\ \text{ps}^2$ and $\ddot{\Phi}_2 = -1660\ \text{ps}^2$, respectively. As shown in Fig. 4(a), the spectra of MLL with pulse repetition rate of 37 MHz (Precision photonics Corp., FFL-1560-B) are at first filtered by TOF1 and TOF2 (Alnair Labs, CVF-220CL) with the same center wavelength of 1555 nm and optical bandwidth of ~4 nm. Then, the center wavelength of TOF2 is detuned by $\sim \pm 0.26$ nm, corresponding to the change of the optical frequency offset between two TOFs from ~ -32 to $\sim +32$ GHz. Note that when the center wavelength of TOF2 changes, the two signals are unaligned in time domain [see Fig. 4(b)]. A VODL (General Photonics, MDL-002) is used to precisely adjust the difference of the time delay between two arms to an integer multiple of the pulse period ($T = 27$ ns).

Figure 5 illustrates three types of the generated microwave waveforms measured by a high-speed real-time oscilloscope (Agilent, DSAX93204A) with 32-GHz bandwidth and 80-GSa/s sampling rate at the output of PD (Finisar, XPDV4120R) and their STFT analyses. It is worth noting that the measured data was subtracted by the averaging data over thousands of times so as to cancel the envelope of the electrical pulses at 37 MHz. Figure 5(a) shows the waveform centered at 0 GHz when the center wavelengths of two TOFs are the same. The measured sweep bandwidth is ~64 GHz (from ~ -32 to ~32 GHz), and the maximum measured instantaneous frequency is ~32 GHz. The pulse duration is ~5.2 ns, corresponding to the sweep rate of $K = \sim 12.3$ GHz/ns. The bandwidth is regarded as ~32 GHz (not ~64 GHz) for calculating the TBWP (= ~166.4) since Eq. (8) is valid for the unidirectional chirp. When the center wavelength of TOF2 is detuned by $\sim \pm 0.26$ nm, the generated down-chirp and up-chirp waveforms are depicted in Figs. 5(c) and 5(e), respectively. As shown in Figs. 5(d) and 5(f), both of the instantaneous frequencies at the middle time locate at ~32 GHz. Their chirp directions are opposite. A significant difference between the generated waveforms and the simulated ones is that only the frequency components within 32 GHz are captured in Figs. 5(d) and 5(f) due to the limited bandwidth of the oscilloscope. The sweep rates (K) are almost the same for all the three types of waveforms, which is consistent with Eq. (9) since K is determined by $\ddot{\Phi}_1$ and $\ddot{\Phi}_2$. The measured waveforms maintain approximately rectangular profiles but have slight amplitude fluctuations. This is possibly caused by the uncertain noise of the PD, the influence of the environment (such as temperature), and the variation of the polarization states of the two arms. More strict study on this factor is now under plan.

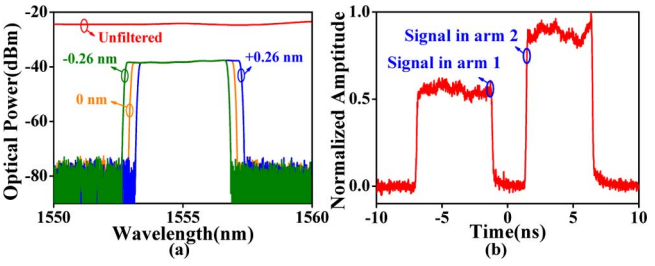

Fig. 4. (a) Optical spectra of MLL and filtered optical spectra when TOF2 is detuned by 0 nm, +0.26 nm, and −0.26 nm. (b) Unaligned pulses in two arms.

In order to quantitatively evaluate the pulse compression of the generated waveforms, we calculated the autocorrelations of the three types of microwave waveforms depicted in Fig. 5. As shown in the zoom-in insets (i) of Figs. 6(a)–6(c), the full width at half-maximum (FWHM) is ~21, ~19, and ~20 ps. Since the effective pulse durations are ~5.2, ~2.6, and ~2.6 ns, the pulse compression ratios ($= T_d/t_{\text{FWHM}}$) equal to ~248, ~137, and ~130, respectively. The FWHM are very close and the pulse compression ratios are almost proportional to TBWP because the maximum instantaneous frequencies of three types of waveforms are all ~32 GHz. Insets (ii) of Figs. 6(a)–6(c) illustrate the normalized intensities under the logarithmic scales. The peak-to-sidelobe ratios (PSLRs) are ~9.0 dB, ~6.4 dB, and ~8.7 dB, respectively.

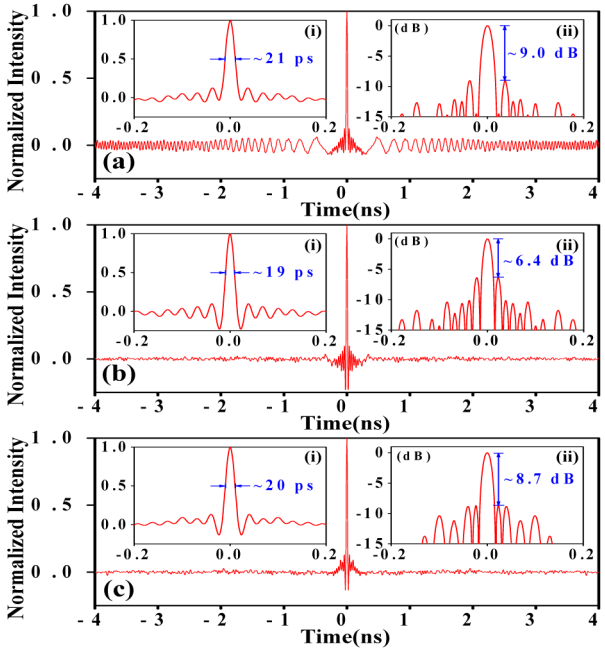

Fig. 6. Autocorrelations of the measured microwave waveforms when the center wavelength of the TOF2 is detuned by (a) 0 nm, (b) +0.26 nm, and (c) −0.26 nm.

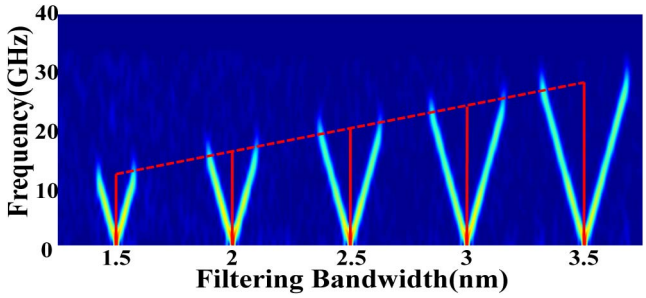

Fig. 7. STFT analyses of the measured microwave waveforms when simultaneously tuning the filtering bandwidths of TOF1 and TOF2 from 1.5 to 3.5 nm.

Furthermore, in order to verify the proportional relationship between the waveform's sweep bandwidth and $\Delta\lambda$, the filtering bandwidths of TOF1 and TOF2 at the same center wavelength of 1555 nm are simultaneously detuned from 1.5 to 3.5 nm. In Fig. 7, the solid lines represent the maximum measured instantaneous frequencies of each filtering bandwidth. As can be seen from the dashed line, the waveforms' sweep bandwidths, being twice of the maximum instantaneous frequency, change almost linearly with $\Delta\lambda$. The experimental observations match well the theoretical analysis given by Eq. (7). Benefiting from the continuous tunability of TOFs, the pulse duration, sweep bandwidth, and TBWP of the generated waveform based on the proposed method can be tuned. Larger sweep bandwidth and TBWP can be achieved by simply increasing $\Delta\lambda$.

In conclusion, we have proposed a method to generate the linearly chirped microwave waveform with tunable center frequency and sweep bandwidth. Experiments are carried out to verify the feasibility of the method. Microwave waveforms with large TBWP and pulse compression ratio have been successfully achieved. Generation of microwave waveforms with larger TBWP can be expected by increasing the TOFs' bandwidth and/or dispersion [see Eq. (8)], which is now under study since it requires a better characterization device.

This work was supported in part by the National Natural Science Foundation of China under Grants 61127016 and 61007052, by the 973 Program under Grant 2011CB301700, by SRFDP of MOE (Grant No. 20130073130005), and by the State Key Lab Project of Shanghai Jiao Tong University under Grant GKZD030033. The authors are grateful to Agilent Technologies co., Ltd. (now Keysight Technologies co., Ltd.) for lending the high-speed real-time oscilloscope.

References

1. M. Skolnik, *Introduction to Radar Systems* (McGraw-Hill, 2001).
2. W. Zou, S. Yang, X. Long, and J. Chen, Opt. Express **23**, 512 (2015).
3. M. Richards, J. Scheer, and W. Holm, *Principles of Modern Radar: Basic Principles* (SciTech, 2010).
4. J. Yao, Opt. Commun. **284**, 3723 (2011).
5. M. Li, J. Azaña, N. Zhu, and J. Yao, Front. Optoelectron. **7**, 359 (2014).
6. W. Li, F. Kong, and J. Yao, J. Lightwave Technol. **31**, 3780 (2013).
7. W. Li and J. Yao, J. Lightwave Technol. **32**, 3573 (2014).
8. J. Chou, Y. Han, and B. Jalali, IEEE Photon. Technol. Lett. **15**, 581 (2003).
9. J. D. McKinney, D. Seo, D. E. Leaird, and A. M. Weiner, J. Lightwave Technol. **21**, 3020 (2003).
10. R. Ashrafi, Y. Park, and J. Azana, IEEE Trans. Microwave Theory Technol. **58**, 3312 (2010).
11. J. H. Wong, H. H. Liu, H. Q. Lam, S. Aditya, J. Zhou, P. H. Lim, K. E. K. Lee, K. Wu, K. K. Chow, and P. P. Shum, Opt. Commun. **304**, 102 (2013).
12. M. Li and J. Yao, IEEE Trans. Microwave Theory Technol. **59**, 3531 (2011).
13. A. Zeitouny, S. Stepanov, O. Levinson, and M. Horowitz, IEEE Photon. Technol. Lett. **17**, 660 (2005).
14. C. Wang and J. Yao, J. Lightwave Technol. **27**, 3336 (2009).
15. H. Gao, C. Lei, M. Chen, F. Xing, H. Chen, and S. Xie, Opt. Express **21**, 23107 (2013).
16. M. A. Muriel, J. Azana, and A. Carballar, Opt. Lett. **24**, 1 (1999).